Journal of CO2 Utilization 69 (2023) 102418

Contents lists available at ScienceDirect

Journal of CO2 Utilization

journal homepage: www.elsevier.com/locate/jcou

Metal recovery from iron slag via pH swing-assisted carbon mineralization with various organic ligands

Sujin Hong [a,1,2], Seokyoon Moon [b,1,3], Gyudae Sim [a,4], Youngjune Park [a,*,5]

[a] School of Earth Sciences and Environmental Engineering, Gwangju Institute of Science and Technology (GIST), 123 Cheomdangwagi-ro, Buk-gu, Gwangju 61005, Republic of Korea
[b] Department of Earth and Environmental Engineering, Columbia University, 500 W. 120th St, New York, NY 10027, United States

ARTICLE INFO

Keywords:
Carbon dioxide
Rare earth element
Acetate
Propionate
Butyrate

ABSTRACT

In this study, we suggest aqueous carbon mineralization of iron slag to selectively produce both solid carbonate and rare earth elements (REEs) under organic ligands such as acetate, propionate, and butyrate, which are the major derivatives of various biogenic wastes. An amorphous phase of iron slag was used as the feedstock, which was confirmed to be quartz and aluminosilicate, and its carbon mineralization was performed with a pH swing-assisted process. When conducting the aqueous carbon mineralization in a series of leaching, precipitation, and carbonation processes by elevating the pH from 3 to 10, all organic ligands exhibited higher leaching efficiencies and recovery yields for all metal species than the inorganic ligand (nitrate). The maximum leaching efficiencies of Ca, and Mg at pH ~ 3 found in acetate were 63.55 and 97.35 wt%, respectively. The total rare earth elements (tREEs) including Y, La, Ce, Pr, and Nd recovered over 50 wt% for all ligands from the pristine iron slag; acetate, propionate, and butyrate exhibited tREEs recovery yields of 54.92, 51.10, and 53.76 wt%, respectively, while nitrate only showed 43.46 wt% in the precipitation step. These metal recovery enhancements are due to the distinct solubility of metal species and their co-precipitation behavior with organic ligands depending on the pH. Owing to the high Ca affinity of the organic ligands, structures of solid carbonates were dominantly controlled as a high-purity calcite, which contained less than 10 ppm of Fe.

1. Introduction

According to the Intergovernmental Panel on Climate Change (IPCC) report on Climate Change in 2021, future CO_2 emission scenarios indicate that net-zero CO_2 emissions must be achieved by the mid-century to limit global temperature rise below 2 °C [1]. Carbon capture, utilization, and storage (CCUS) technologies – capturing, separating, transporting, converting, and storing CO_2 that is generated from industrial sectors – have been recognized as a promising option toward net-zero CO_2 emissions [2,3]. Among the CCUS technologies, ex-situ carbon mineralization technology that artificially transforms CO_2 into solid carbonates (e.g., $CaCO_3$, and $MgCO_3$) with alkali earth metals (e.g., Ca or Mg), is generally performed through gas-solid or aqueous systems, which aim to accomplish large-scale CO_2 storage and utilization [4,5]. Either natural silicate minerals (e.g., wollastonite, basalts, olivine, and serpentine) or alkaline industrial wastes (e.g., iron and steel slags, mine tailings, gypsums, coal ashes, construction wastes, etc.) have been considered as the feedstock to provide alkali earth metals [6,7]. Since solid carbonate has the most thermodynamically stable energy level among the carbon-derivative compounds, it can permanently sequestrate CO_2 while relieving the critical issue of CO_2 leakage in the geological CO_2 injection approach [4,8]. Moreover, solid carbonates can be used in various industries such as adhesives, sealants, food and pharmaceuticals, paints, coatings, paper, cements, and construction materials [9–11], thereby also contributing to realizing a circular carbon economy. Even though various approaches to ex-situ carbon mineralization

* Corresponding author.
E-mail address: young@gist.ac.kr (Y. Park).
[1] These authors contributed equally to this work.
[2] ORCID: 0000-0001-9114-2722.
[3] ORCID: 0000-0002-1608-5809.
[4] ORCID: 0000-0003-3395-0099.
[5] ORCID: 0000-0001-5626-0563.

https://doi.org/10.1016/j.jcou.2023.102418
Received 15 November 2022; Received in revised form 27 January 2023; Accepted 30 January 2023

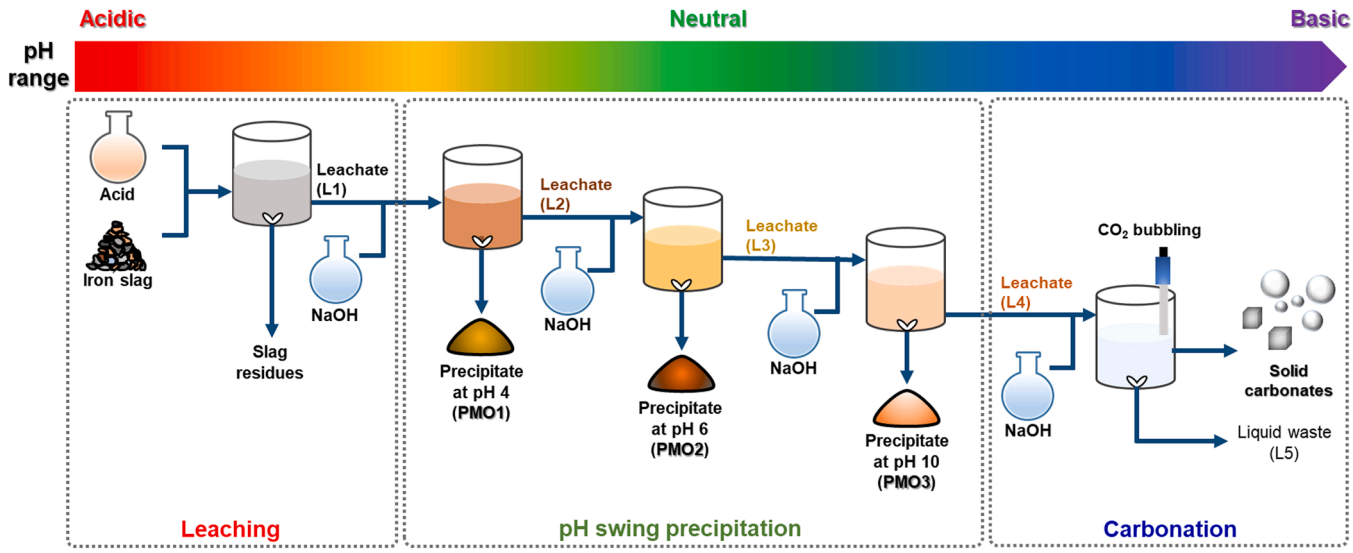

Fig. 1. Scheme of aqueous pH swing-assisted carbon mineralization process for polygeneration of high-purity solid carbonates and rare earth elements.

technology have been proposed over the past few decades [12–14], their current status still resides in a wide range of technology readiness levels (TRL) from 3 to 9 [5,8], due to some remaining challenges; for example, (i) there are limited quantities of highly reactive feedstocks in some regions or countries, (ii) the reaction system often shows high complexity, and (iii) the product market is still uncertain [3,6].

To accelerate the large-scale implementation of ex-situ carbon mineralization, understanding the complexity of bulk feedstock, enhancing reaction kinetics and carbonation efficiency, and producing high value-added materials were suggested as breakthroughs to overcome the current bottleneck [3,15–18]. Because alkaline industrial wastes generally exhibit cheaper cost, higher reactivity, and better accessibility to CO_2 sources than natural silicate minerals, its successful implementation can accomplish both waste treatment and value-added production; thus, alkaline industrial wastes have been recognized as promising feedstock to meet these breakthroughs [5,7].

In this study, to make the ex-situ carbon mineralization process more feasible, we focused on the novel carbon mineralization process with polygeneration, specifically producing both high-purity $CaCO_3$, and rare earth elements (REEs)-concentrated precipitated metal oxides, which could be an alternative natural REE ore. REEs consist of seventeen kinds of metal elements including fifteen lanthanides, yttrium (Y), and scandium (Sc) [19], and are key elements used in various industries including electric devices and green technologies [20]. The global demand for REEs is expected to grow rapidly, but the uncertainty of its supply chain still remains. Note that REEs are only reserved to a few countries (e.g., China, Australia, Canada, and the United States); thus, many other countries such as Republic of Korea rely on the import of REEs to meet their demand [19]. To manage the high risk of REE supply, its recovery from electrical device wastes and other industrial wastes are being actively studied, and recent literature has reported that bulk industrial wastes such as coal ashes, and iron slag, which contain REEs over a few hundred ppm levels, can be an alternative REE ore via concentrating REEs up to the current ore-grade level [19,21,22].

Our previous study introduced a multi-step pH swing-assisted carbon mineralization process using inorganic acids, which can not only enhance reaction kinetics but also produce value-added materials (e.g., high-purity $CaCO_3$) [5,21]. From these results, we newly presented the concept of simultaneous selective REE recovery and CO_2 storage via an aqueous carbon mineralization. However, the carbon mineralization process is costly due to requiring a large amount of inorganic solvents [21]. In general, 50% of the carbon mineralization process cost in the aqueous phase corresponds to the solvent consumed [23]. To relieve these costs, volatile organic acids (VOAs) generated by anaerobic digestion of biogenic wastes were investigated as the leaching solvent of steel slag in a differential bed reactor [24]. Owing to the strong stability constants between organic ligands and metal ions [25], VOAs including acetic acid, propionic acid, butyric acid, valeric acid, and their mixture showed better leaching efficiencies and faster reaction kinetics for metal elements than inorganic acids (i.e., HCl and HNO_3) at the same pH condition. These indicate that an aqueous carbon mineralization process integrated with the biogenic waste streams is feasible [24].

Here, we conducted an aqueous carbon mineralization process with REE recovery from iron slag under organic ligands (e.g., acetate, propionate, and butyrate) aiming to newly establish the waste-to-resource supply chain. The results were compared with the case of inorganic ligand (HNO_3). As shown in Fig. 1, this process was constructed via a series of steps including leaching, three-steps pH swing-assisted precipitation, and carbonation with CO_2. Iron slag was used as feedstock, and its physicochemical properties were characterized. The dissolution and precipitation behaviors of the metal species shown in each step were explored. REE recovery behavior according to ligand type was obtained. Finally, the obtained high-purity $CaCO_3$ was characterized.

2. Materials and methods

2.1. Materials

Iron slag, supplied by POSCO (Pohang, Republic of Korea), was used as the feedstock controlled with a particle size (d_p) ranging from 54 to 200 μm. Nitric acid (HNO_3, 68–70%), sodium hydroxide (NaOH, 97%, pellets), and organic ligand salts including sodium acetate (99%, CH_3COONa), sodium propionate (99%, CH_3CH_2COONa), and sodium butyrate (98%, CH_3CH_2 CH_2COONa) were purchased from Sigma Aldrich, Inc. (USA). CO_2 gas purified to 99.99% was provided by Daedeok Gas Co., Ltd (Republic of Korea). Purified water was provided from a water purification system (HIQ-I, Coretech Co., Ltd., Republic of Korea).

2.2. Experimental procedure of aqueous carbon mineralization

An aqueous carbon mineralization experiment consisting of leaching, three-steps pH swing precipitation, and carbonation by bubbling CO_2 was conducted in a batch reactor system at 25 °C. Metal leaching from iron slag was performed in a 0.3 L solution at 1/8 of the solid to liquid (acid) ratio (S/L ratio, kg/L) for 2 h. For the inorganic ligand

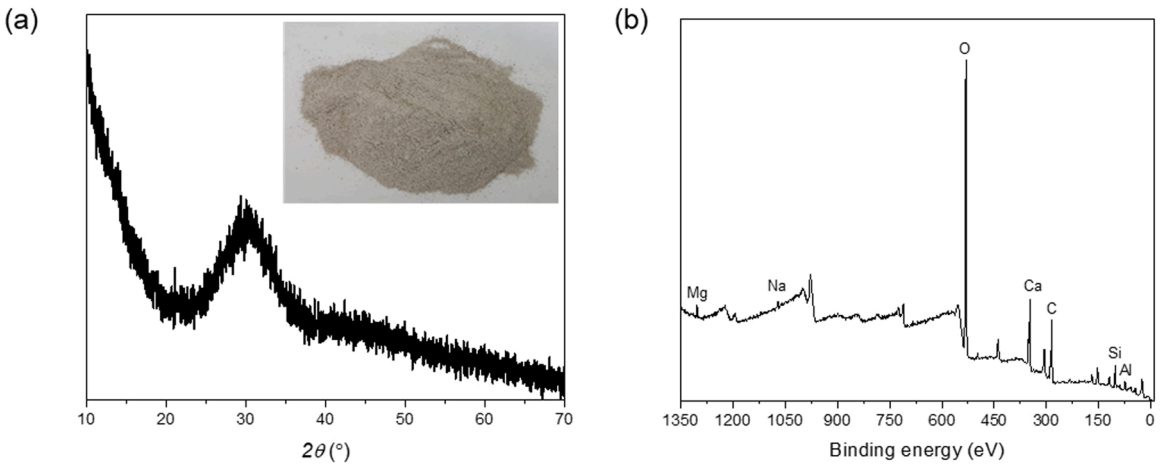

Fig. 2. (a) PXRD pattern and (b) XPS spectrum of the iron slag used in this study.

(hereafter, NA), 0.001 M of HNO_3 solution was prepared, which was pH 3. For the organic ligands, solutions containing 0.001 M of HNO_3 and 0.05 M of sodium acetate (hereafter, NA-Ac), sodium propionate (hereafter, NA-Prop), or sodium butyrate (hereafter, NA-But) were prepared. During the leaching process, the stirring was set to 700 rpm, the pH of the slurry was maintained at ~ 3, and was monitored using a pH meter (S220, Mettler-Toledo International Inc., USA). The leachates (L1) recovered after leaching were used as a reactant in the next step.

To selectively concentrate metal species dissolved in L1, the pH swing precipitation was conducted by stepwise increasing of the pH to 4, 6, and 10 with NaOH. The recovered precipitated metal oxides in each pH step were named as PMO1 (at pH 4), PMO2 (at pH 6), and PMO3 (at pH 10). The corresponding leachates (L2 at pH 4 and L3 at pH 6) were also produced. These leachates were provided for the next pH step. While each precipitation step was maintained with a stirring rate of 200 rpm for 1 h, pH was adjusted by adding NaOH.

Carbonation was performed by injecting gaseous CO_2 into the leachate (L4) recovered after precipitation at pH 10. The pH was controlled between 10 and 11 by injecting NaOH, and the stirring rate was set to 200 rpm, maintaining 10 L/min of CO_2 flow rate for 0.5 h. Solid carbonates were then separated from the leachate (L5), and washed using purified water. All slurries recovered after each step were separated into leachates and solid residues by a vacuum filtration system equipped with 0.45 μm of filter paper. Finally, these solids were collected after drying at 70 °C in a convection oven (OF-02 GW, Jeio Tech Co., Ltd., Republic of Korea) for 24 h.

2.3. Characteristic analyses

The chemical composition of iron slag including both major and trace metals was determined by using inductively coupled plasma—mass spectrometry (ICP—MS, 7900, Agilent Technologies, Inc., USA), inductively coupled plasma—optical emission spectroscopy (ICP—OES, OPTIMA 8300, PerkinElmer, Inc., USA), and an X-ray fluorescence spectrometer (XRF, Axios FAST, Malvern Panalytical Ltd., UK). To completely convert iron slag to be dissolved before the ICP measurements, the iron slag powder (~ 0.2 g) was ground in a mill before being added to 10 mL of HCl solution at 90 °C for 6 h. The prepared solution was then put into a mixture of HNO_3, hydrofluoric acid (HF), and hydrogen peroxide (H_2O_2), which was digested for 10 min in a microwave digestion system (TOPEX+, Preekem Scientific Instruments Co., Ltd., China). The liquid sample filtered using a 0.45 μm syringe filter was diluted with a 1% HNO_3 solution.

To explore the dissolution and precipitation behaviors of the metal species as a function of pH, aliquots (1 mL) of the leachates collected at all steps and dried solid samples (0.2 g) were completely dissolved in 4 mL of aqua regia. These liquid samples were diluted to 10 mL of 2% HNO_3 solution, and their elemental concentrations were measured by ICP—OES and ICP—MS. The leaching efficiency and conversion ratio of metal species were calculated using Eqs. (1) and (2), respectively, as follows:

$$\text{Leaching efficiency of metal specie} = \frac{C_{L1,i} \times V_{L1}}{C_{s,i} \times m_s} \times 100(\text{wt\%}) \quad (1)$$

$$\text{Residual elemental fraction in leachate} = \frac{C_{L,i} \times V_L}{C_{L1,i} \times V_{L1}} (L = L1, L2, L3, L4, or L5) \quad (2)$$

where $C_{s,i}$ (mg/kg) and m_s (kg) indicate the concentration of element i and total mass of iron slag, respectively. $C_{L1,i}$ (mg/L) and V_{L1} (L) are the concentration of element i in the *L1* and leachate volume of *L1*, respectively. $C_{L,i}$ (mg/L) and V_L (L) express the concentration of element i in the leachate of *L1, L2, L3, L4 or L5*, and each leachate volume, respectively.

Particle properties of solids including the raw iron slag, solid residues, precipitated metal oxides, and solid carbonate were investigated by a particle size analyzer (PSA, LS 13 320 MW, Beckman Coulter, Inc., USA), X-ray photoelectron spectroscopy (XPS, NEXSA, Thermo Fisher Scientific Inc., USA), field emission—scanning electron microscope (FE—SEM, S-4700, Hitachi Ltd., Japan), and powder X-ray diffractometer (PXRD, SmartLab, Rigaku, Co., Japan). The diffraction patterns were obtained in the 2θ range of 10 – 70° (0.02° step size) using CuKα radiation ($\lambda = 1.5406$ Å) with a 2 kW generator. Rietveld refinement was conducted by using FullProf software [26].

A thermogravimetric analyzer (TGA, TGA-50, Shimadzu Scientific Instruments, Inc., Japan) was used for the characterization of the precipitated $CaCO_3$. The TGA system was run in a temperature range from ambient to 900 °C with a 10 °C/min heating rate under N_2 gas.

3. Results and discussion

3.1. Characterization of iron slag

Iron slag generally represents a high complexity in mineralogical structure and chemical composition, which affects the reaction mechanism, leaching kinetics, reactivity, etc [27]. Thus, mineralogical structure and chemical composition of the raw iron slag were investigated prior to conducting aqueous carbon mineralization under various ligands. The mineralogical structure of the iron slag was examined by PXRD analysis. As shown in Fig. 2(a), the PXRD pattern showed only a large bump that is typically illustrated to be an amorphous phase [24, 28]. The detailed elemental arrangement in this amorphous phase was

Table 1
Elemental compositions of iron slag.

Major elements, wt%					
Ca	Si	Mg	Al	Fe	Others
25.08	14.42	3.62	6.05	0.49	50.34
Rare earth elements (REEs), ppm					
La	Ce	Pr	Nd	Y	Total REEs (tREEs)
73.6	151.6	17.4	68.1	80.9	391.6

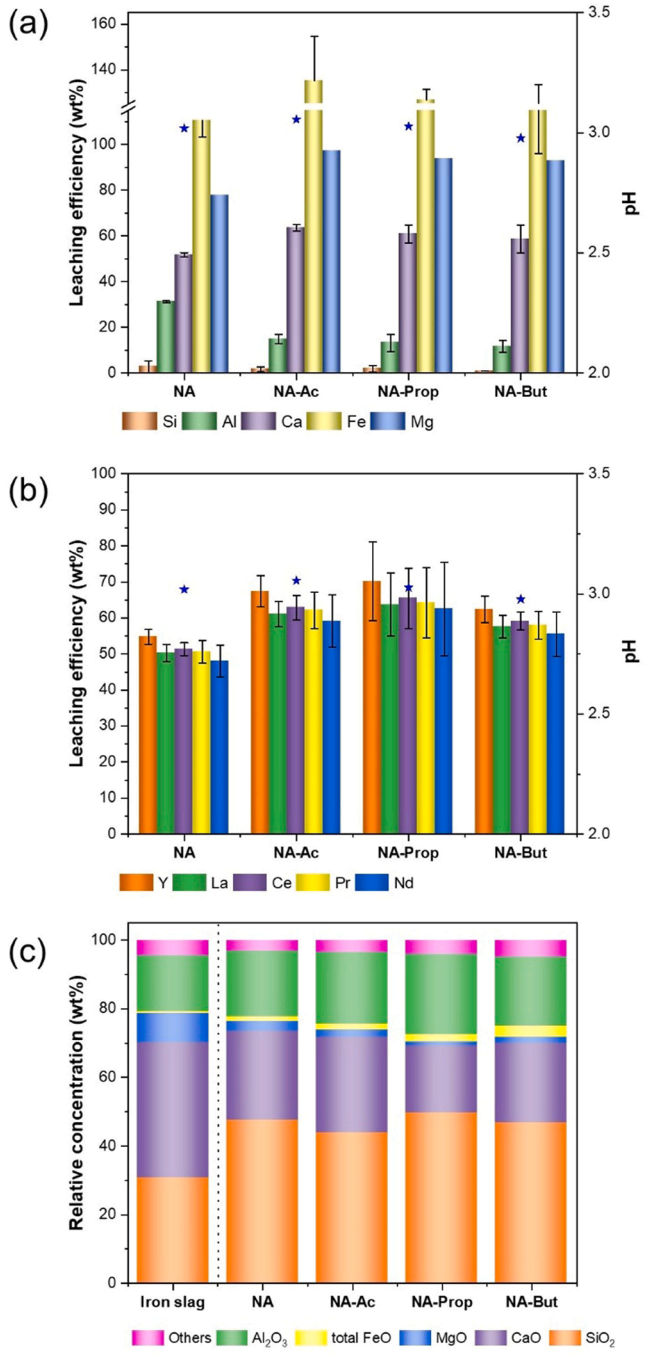

Fig. 3. Leaching efficiency of (a) major elements and (b) REEs from raw iron slag at S/L (kg/L) = 1/8 at 25 °C. (c) Relative composition of solid residues recovered after leaching.

also explored using the XPS spectrum shown in Fig. 2(a). The binding energies of Al(2p) and Si(2p) were 74.28 and 102.11 eV, respectively, and it is postulated that the iron slag consists of the aluminosilicate and quartz structures (Fig. 2(b)) [29].

To determine the concentrations of major metals and REEs in the raw iron slag, the chemical composition using ICP—OES and ICP—MS was measured. As shown in Table 1, the iron slag exhibited the chemical composition of both major metals and REEs regardless of particle sizes, and it consisted of Ca (25.08 wt%), Si (14.43 wt%), Al (6.05 wt%), Mg (3.62 wt%), and Fe (0.49 wt%) as the major metals. The total rare earth elements (tREEs) were 391.6 ppm, including lanthanum (La), cerium (Ce), praseodymium (Pr), neodymium (Nd), and Y.

3.2. Iron slag leaching under inorganic and organic ligands

Major elements and REEs from the raw iron slag were first leached under inorganic and organic ligand conditions. Leaching of the iron slag depending on the oxidation state of metal species can be expressed as follows:

$$2HA + \text{iron slag} \leftrightarrow 2H^+ + DA_2 \ (D = \text{divalent metal species such as } Ca^{2+}, Mg^{2+}, Fe^{2+}) \quad (3)$$

$$3HA + \text{iron slag} \leftrightarrow 3H^+ + T_2A_3 \ (T = \text{trivalent metal species such as } Al^{3+}, Fe^{3+}, REE^{3+}) \quad (4)$$

($A = NO_3^-$, CH_3COO^-, $C_2H_5COO^-$, and $C_3H_7COO^-$).

As shown in Fig. 3(a) and (b), the organic ligands improved the leaching efficiencies of both major metals and REEs more than those of the inorganic ligand (NA) at the same pH condition. Interestingly, Si leaching efficiency was shown below 10 wt% regardless of ligand type. This could be due to its re-precipitation at the pH condition. To identify the Si re-precipitation during leaching, the relative composition of solid residues obtained in the leaching step was analyzed by XRF (Fig. 3(c)). Compared to the raw iron slag, Si concentration in the solid residues increased by about 10%. Previous literature explained that silicates dissolved in an acidic environment form silicic acids as the building block of silica, and those acids are stable at pH 2; however, they may be condensed into silicas by polymerization or precipitation in the amorphous phase by increasing the pH [30,31]. Note that Si is saturated and precipitates above 132 ppm (SiO_2) at 20 °C [32]. Again, the iron slag leaching under inorganic and organic ligands was also performed at 1/1000 of the S/L ratio, and Si leaching efficiencies ranged from 82.92 to 89.42 wt% (Fig. S1). From this evidence, we speculated that Si leached at 1/8 of the S/L ratio was polymerized and recovered with slag residues. Regardless of ligand type, slag residues also showed an amorphous phase as shown in the PXRD patterns (Fig. S2(a)). Furthermore, they exhibited white particles with a wider particle size distribution than the iron slag (Fig. S2 (b) and (c)).

3.3. Three-step pH swing for recovering rare earth elements

Metal species dissolved in an aqueous solution can be precipitated according to its thermodynamic solubility as a function of pH [25]. To selectively concentrate REEs and liberate alkali metals (e.g., Ca and Mg), three-step pH swing-assisted precipitations at pH 4, 6, and 10 were conducted using the L1 leachate generated by the case of 1/8 of the S/L ratio. The pH was controlled by adding NaOH. The pH swing-assisted precipitation of the metal species is represented as follows:

$$DA_2 + 2NaOH \leftrightarrow D(OH)_2 + 2NaA \quad (5)$$

$$T_2A_3 + 3NaOH \leftrightarrow T(OH)_3 + 3NaA \quad (6)$$

Fig. 4 shows the residual elemental fraction of each leachate under inorganic and organic ligands. This pattern shows how much of each element including REEs remained or precipitated out during the pH swing steps. The Al and Fe species were mostly precipitated and

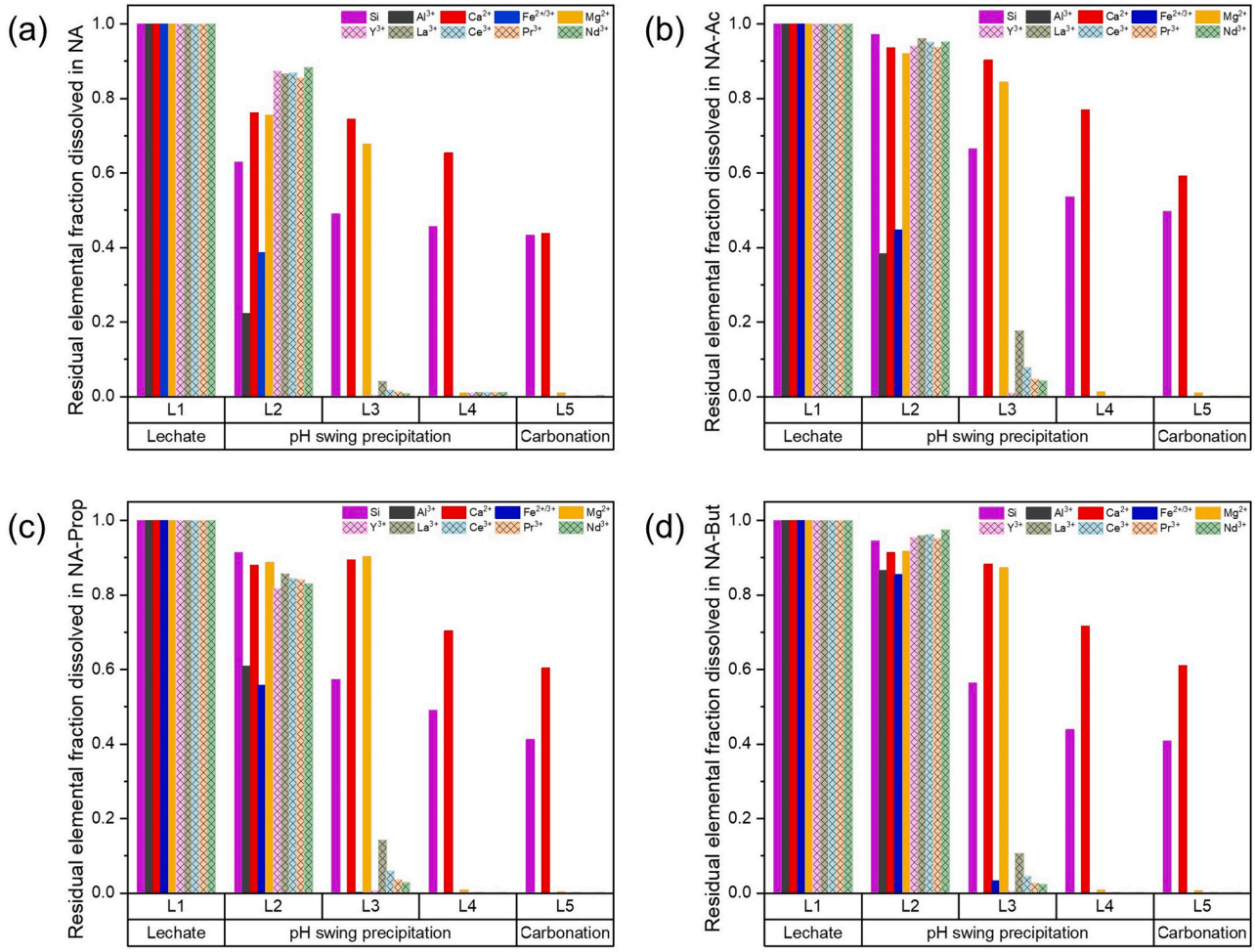

Fig. 4. Residual elemental fraction of each leachate generated by (a) NA, (b) NA-Ac, (c) NA-Prop, and (d) NA-But.

Table 2
Leaching efficiency, recovered tREEs, and $CaCO_3$ purity.

Ligand	Chemicals	Leaching efficiency (wt %)	Recovered tREEs (wt%)	$CaCO_3$ purity (wt %)
NA	HNO_3 / NaOH	Ca: 51.68 Mg: 77.78 tREEs: 50.98	43.46	95.30
NA-Ac	HNO_3 / Na-acetate / NaOH	Ca: 63.55 Mg: 97.35 tREEs: 62.54	54.92	93.61
NA-Prop	HNO_3 / Na-propionate / NaOH	Ca: 60.84 Mg: 93.80 tREEs: 65.20	51.10	94.10
NA-But	HNO_3 / Na-butyrate / NaOH	Ca: 58.63 Mg: 92.97 tREEs: 58.51	53.76	94.00

removed at a pH between pH 4 (L2) and 6 (L3). However, the organic ligands (e.g., NA-Ac, NA-Prop, and NA-But) removed less Al and Fe species from the L1 than the NA case possibly due to the high stability constant between the metal ions and organic ligands. Regardless of ligand type, pH 10 (L4) favorably removed the Mg-bearing precipitate. In all cases, most of the REEs were concentrated as the precipitates at pH 6 (PMO2). The recovery fraction of the tREEs from the L1 by NA, NA-Ac, NA-Prop, and NA-But at pH 6 (PMO2) was 85.25, 87.82, 78.38, and 91.89 wt%, respectively. This indicates that the use of organic ligands recovered over the half of the tREEs in the raw iron slag as a solid residue

Table 3
Concentration of REEs in PMO2.

Ligand	Rare earth elements (ppm)					
	Y	La	Ce	Pr	Nd	tREEs
NA	885.5	676.9	1438	165.0	638.8	3804.2
NA-Ac	1141	927.8	1980	225.4	879.6	5153.8
NA-Prop	977.7	471.9	1296	161.5	645.8	3552.9
NA-But	768.5	419.6	1097	132.1	519.9	2937.1

in the precipitation step as 54.92, 51.10, and 53.76 wt% for NA-Ac, NA-Prop, NA-But, respectively: higher than the use of NA (Table 2). Table 3 shows the concentrations of tREEs in the PMO2 for NA, NA-Ac, NA-Prop, and NA-But. The NA-Ac case exhibited the highest tREEs concentration of 5153.8 ppm. Note that the initial REEs concentration in the iron slag was 391.6 ppm. Fig. S3 presents PMOs recovered during pH swing-assisted precipitation from pH 4–10. It appears that the distinct colors of the solid residues rely on pH and their oxidation states [33].

3.4. Synthesis of solid carbonate and its properties

Carbonation was finally performed by injecting CO_2 gas into the L4 leachate in which Ca was the major species. Solid carbonation can occur by the reaction with CO_2 as described below:

$$CO_2 + H_2O \leftrightarrow H_2CO_3 \quad (7)$$

$$H_2CO_3 + NaOH \leftrightarrow HCO_3^- + H_2O + Na^+ \quad (8)$$

Table 4
Impurities of precipitated $CaCO_3$.

Sample	Elements (ppm)			
	Mg	Fe	Si	Al
NA	489.3	7.7	1172.8	-
NA-Ac	1564	-	1188	-
NA-Prop	1674.1	3.7	1207.4	-
NA-But	743.4	11.3	1256.6	-

Table 5
Structural properties of precipitated $CaCO_3$ under various ligand types.

		NA	NA-Ac	NA-Prop	NA-But
Lattice parameter of calcite (Å)	*a*	4.9932	4.9964	5.002	4.996
	b	4.9932	4.9964	5.002	4.996
	c	17.0612	17.0793	17.083	17.083
Polymorph (%)	Calcite (hexagonal, $R\bar{3}2/c$)	100	96.23	92.95	93.7
	Vaterite (hexagonal, $P6_3/mmc$)	0	3.77	7.05	6.3

$$HCO_3^- + NaOH \leftrightarrow CO_3^{2-} + H_2O + Na^+ \quad (9)$$

$$(Mg^{2+}, Ca^{2+})A_2 + CO_3^{2-} + 2Na^+ \leftrightarrow (Mg/Ca)CO_3 + 2NaA \quad (10)$$

Solid carbonates recovered after carbonation were confirmed as $CaCO_3$ with a purity > 93% for all organic ligands, which was analyzed by TGA (Fig. S4). The minor impurities in the $CaCO_3$ were also analyzed using ICP—MS, and the results are given in Table 4. Interestingly, Fe was detected to be less than 12 ppm in all solid carbonates.

$CaCO_3$ is known to form various polymorphs including amorphous, hydrous crystals (e.g., monohydrocalcite and ikaite), and anhydrous crystals (e.g., calcite, aragonite, and vaterite) [34,35]. Since those $CaCO_3$ structures exhibit different physicochemical properties (e.g., density, morphology, and particle size) which are controlled under various conditions such as pH, reaction time, additive, temperature, solute concentration, and solvent type [2,36], the crystalline structures of the synthesized $CaCO_3$ in the presence of various ligands were also examined using PXRD refinements (Fig. S5 and Table 5). Since complexes between Ca and ligand stabilize unstable $CaCO_3$ which induces the transformation into calcite [36], all $CaCO_3$ were dominantly crystallized to calcite; however, the larger ligands formed an unstable structure (i.e., vaterite). Calcite morphologies also differed depending on the ligand type, and increasing ligand size induced the formation of elongated spheroids, as shown in Fig. 5. Previous studies described that organic additives can induce the formation of elongated spheroids because complexes between the Ca and ligand interact with the calcite face, which limits crystal growth on the surface [36,37].

4. Conclusions

This study conducted selective polygeneration of both $CaCO_3$ and REEs via aqueous carbon mineralization of iron slag in a series of leaching, pH swing-assisted precipitation from pH 4–10, and carbonation with CO_2. The solvents used in this process were organic ligands which can be derived from various biogenic wastes. When conducting the aqueous carbon mineralization in a series of leaching, precipitation, and carbonation processes with elevating pH from 3 to 10, all organic ligands exhibited higher leaching efficiencies and recovery yields for all

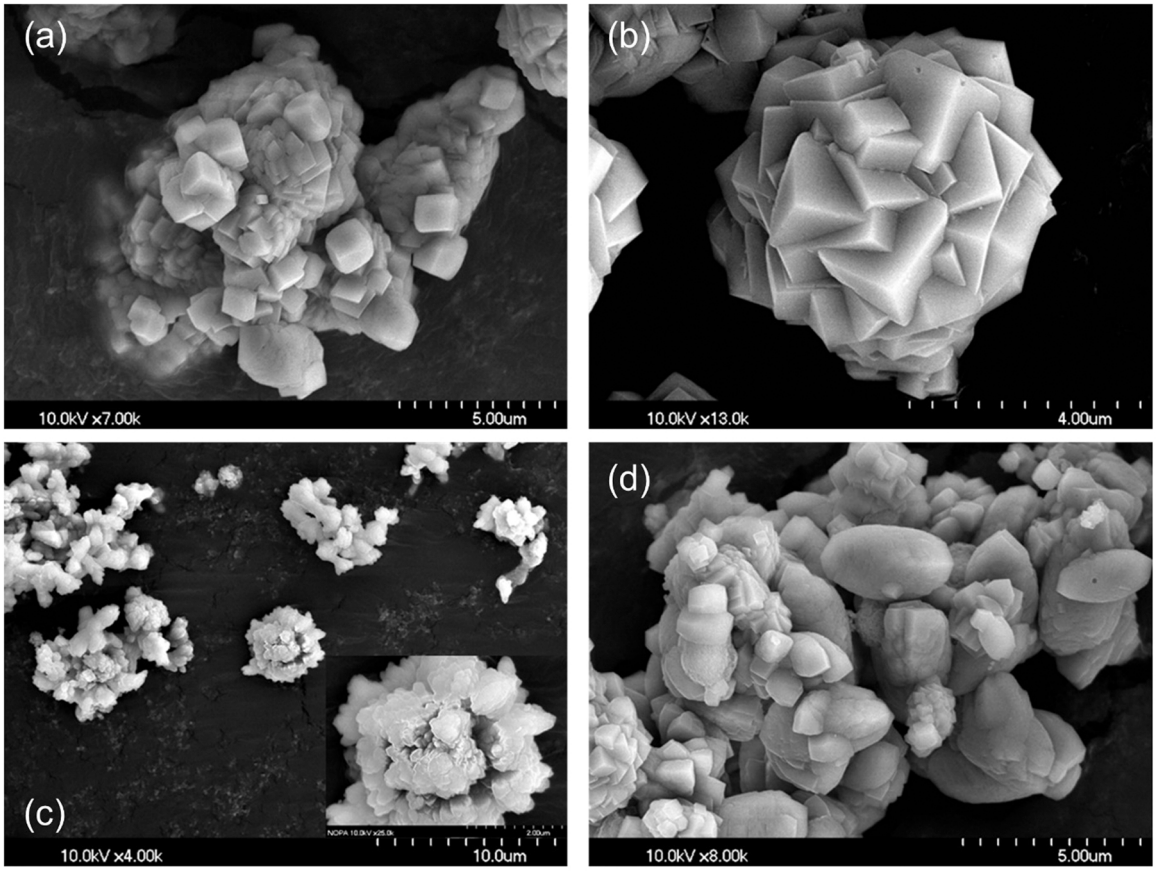

Fig. 5. SEM images of precipitated $CaCO_3$ obtained from (a) NA, (b) NA-Ac, (c) NA-Prop, and (d) NA-But.

metal species than inorganic ligand (nitrate). Specifically, the maximum leaching efficiencies of Ca, and Mg at pH ~ 3 were found in acetate, as 63.55 and 97.35 wt%, respectively. The tREEs, including Y, La, Ce, Pr, and Nd, recovered over 50 wt% for all ligands from the pristine iron slag; acetate, propionate, and butyrate exhibited tREEs recovery yields of 54.92, 51.10, and 53.76 wt%, respectively, while the nitrate only showed 43.46 wt% in the precipitation step. This metal recovery enhancement is due to the distinct solubility of metal species and their co-precipitation behavior with organic ligands depending on pH. $CaCO_3$ produced with a purity > 93% were mainly controlled as calcite because the high Ca affinity of ligands induces the transformation of unstable $CaCO_3$ to calcite. Even though the aqueous carbon mineralization process proposed should be further studied for improving process performances and understanding reaction complexity induced by waste streams, this work provides insight for newly establishing the waste-to-supply chain toward a circular carbon economy as well as net-zero CO_2 emissions.

Synopsis

This study provides insight for newly establishing the waste-to-supply chain toward a circular economy as well as net-zero CO_2 emissions.

CRediT authorship contribution statement

Sujin Hong: Conceptualization, Validation, Investigation, Writing – original draft. **Seokyoon Moon**: Conceptualization, Validation, Formal analysis, Writing – review & editing, Visualization. **Gyudae Sim**: Conceptualization, Methodology, Investigation, Data curation. **Youngjune Park**: Writing – review & editing, Supervision, Project administration, Funding acquisition.

Author contributions

The manuscript was written through contributions of all authors.

Declaration of Competing Interest

The authors declare that they have no known competing financial interests or personal relationships that could have appeared to influence the work reported in this paper.

Data availability

Data will be made available on request.

Acknowledgments

This work was supported by Korea Institute of Energy Technology Evaluation and Planning (KETEP) grant funded by the Korea government (MOTIE) (No. 20188550000580). This work also was supported by the GIST Research Project grant funded by the GIST in 2023. We are also grateful to Dr. SangHo Yi (POSCO) for the valuable comments on this study.

Appendix A. Supplementary material

Supplementary data associated with this article can be found in the online version at doi:10.1016/j.jcou.2023.102418.

References

[1] IPCC, Climate Change 2021: The Physical Science Basis. Contribution of Working Group I to the Sixth Assessment Report of the Intergovernmental Panel on Climate Change, 2021.
[2] R. Chang, D. Choi, M.H. Kim, Y. Park, Tuning crystal polymorphisms and structural investigation of precipitated calcium carbonates for CO_2 mineralization, ACS Sustain. Chem. Eng. 5 (2) (2017) 1659–1667, https://doi.org/10.1021/acssuschemeng.6b02411.
[3] Mission Innovation, Accelerating Breakthrough Innovation in Carbon Capture Utilization and Storage, Department of Energy, 2017.
[4] W. Liu, L. Teng, S. Rohani, Z. Qin, B. Zhao, C.C. Xu, S. Ren, Q. Liu, B. Liang, CO_2 mineral carbonation using industrial solid wastes: a review of recent developments, Chem. Eng. J. 416 (2021), https://doi.org/10.1016/j.cej.2021.129093.
[5] N. Zhang, Y.E. Chai, R.M. Santos, L. Šiller, Advances in process development of aqueous CO_2 mineralisation towards scalability, J. Environ. Chem. Eng. 8 (6) (2020), https://doi.org/10.1016/j.jece.2020.104453.
[6] S.-Y. Pan, Y.-H. Chen, L.-S. Fan, H. Kim, X. Gao, T.-C. Ling, P.-C. Chiang, S.-L. Pei, G. Gu, CO_2 mineralization and utilization by alkaline solid wastes for potential carbon reduction, Nat. Sustain 3 (5) (2020), https://doi.org/10.1038/s41893-020-0486-9.
[7] A. Sanna, M. Uibu, G. Caramanna, R. Kuusik, M.M. Maroto-Valer, A review of mineral carbonation technologies to sequester CO_2, Chem. Soc. Rev. 43 (23) (2014) 8049–8080, https://doi.org/10.1039/C4CS00035H.
[8] A.D.N. Kamkeng, M. Wang, J. Hu, W. Du, F. Qian, Transformation technologies for CO_2 utilisation: current status, challenges and future prospects, Chem. Eng. J. 409 (2021), https://doi.org/10.1016/j.cej.2020.128138.
[9] R. Chang, S. Kim, S. Lee, S. Choi, M. Kim, Y. Park, Calcium carbonate precipitation for CO_2 storage and utilization: a review of the carbonate crystallization and polymorphism, Front. Energy Res. 5 (2017) 17, https://doi.org/10.3389/fenrg.2017.00017.
[10] S. Hong, G. Sim, S. Moon, Y. Park, Low-temperature regeneration of amines integrated with production of structure-controlled calcium carbonates for combined CO_2 capture and utilization, Energy Fuels 34 (3) (2020), https://doi.org/10.1021/acs.energyfuels.9b04339.
[11] A. Botha, C.A. Strydom, Preparation of a magnesium hydroxy carbonate from magnesium hydroxide, Hydrometallurgy 62 (3) (2001) 175–183, https://doi.org/10.1016/S0304-386X(01)00197-9.
[12] J.-H. Bang, S.-C. Chae, K. Song, S.-W. Lee, Optimizing experimental parameters in sequential CO_2 mineralization using seawater desalination brine, Desalination 519 (2021), https://doi.org/10.1016/j.desal.2021.115309.
[13] X. Wang, M.M. Maroto-Valer, Integration of CO_2 capture and mineral carbonation by using recyclable ammonium salts, ChemSusChem 4 (9) (2011) 1291–1300, https://doi.org/10.1002/cssc.201000441.
[14] A.-H.A. Park, L.-S. Fan, CO_2 mineral sequestration: physically activated dissolution of serpentine and pH swing process, Chem. Eng. Sci. 59 (22) (2004) 5241–5247, https://doi.org/10.1016/j.ces.2004.09.008.
[15] M. Owais, M. Järvinen, P. Taskinen, A. Said, Experimental study on the extraction of calcium, magnesium, vanadium and silicon from steelmaking slags for improved mineral carbonation of CO_2, J. CO_2 Util. 31 (2020) 1–7, https://doi.org/10.1016/j.jcou.2019.02.014.
[16] Minyu He, Liumei Teng, Yuxiang Gao, Sohrab Rohani, Shan Ren, Jiangling Li, Jian Yang, Qingcai Liu, Weizao Liu, Simultaneous CO_2 mineral sequestration and rutile beneficiation by using titanium-bearing blast furnace slag: process description and optimization, Energy 248 (2022), https://doi.org/10.1016/j.energy.2022.123643.
[17] Guang Hu, Sohrab Rohani, Xiaoyong Jiang, Jiangling Li, Qingcai Liu, Weizao Liu, CO_2 mineral sequestration and faujasite zeolite synthesis by using blast furnace slag: process optimization and CO_2 net-emission reduction evaluation, ACS Sustain. Chem. Eng. 9 (41) (2021) 13963–13971, https://doi.org/10.1021/acssuschemeng.1c05576.
[18] Weizao Liu, Tahani Aldahri, Chunbao Xu, Chun Li, Sohrab Rohani, Synthesis of sole gismondine-type zeolite from blast furnace slag during CO_2 mineralization process, J. Environ. Chem. Eng. 9 (1) (2021), 104652, https://doi.org/10.1016/j.jece.2020.104652.
[19] B.A. Herbert Cooper, 21st Century Products: A Challenging Economic Future, American Institute of Chemical Engineers, 2018.
[20] P. Rasoulnia, R. Barthen, A.-M. Lakaniemi, A critical review of bioleaching of rare earth elements: the mechanisms and effect of process parameters, Crit. Rev. Environ. Sci. Technol. 51 (4) (2021) 378–427, https://doi.org/10.1080/10643389.2020.1727718.
[21] G. Sim, S. Hong, S. Moon, S. Noh, J. Cho, P.T. Triwigati, A.-H.A. Park, Y. Park, Simultaneous CO_2 utilization and rare earth elements recovery by novel aqueous carbon mineralization of blast furnace slag, J. Environ. Chem. Eng. 10 (2) (2022), https://doi.org/10.1016/j.jece.2022.107327.
[22] G. Jeong, S. Kim, K. Kim, Rare metal chemistry, microstructures, and mineralogy of coal ash from thermal power plants of Korea, J. Miner. Soc. Korea 28 (2) (2015) 147–163, https://doi.org/10.9727/jmsk.2015.28.2.147.
[23] S. Giannoulakis, K. Volkart, C. Bauer, Life cycle and cost assessment of mineral carbonation for carbon capture and storage in European power generation, Int. J. Greenh. Gas Control 21 (2014) 140–157, https://doi.org/10.1016/j.ijggc.2013.12.002.
[24] S. Hong, H.D. Huang, G. Rim, Y. Park, A.-H.A. Park, Integration of two waste streams for carbon storage and utilization: enhanced metal extraction from steel slag using biogenic volatile organic acids, ACS Sustain. Chem. Eng. 8 (50) (2020) 18519–18527, https://doi.org/10.1021/acssuschemeng.0c06355.
[25] M.M. Benjamin. Water Chemistry, second ed., Waveland Press, 2014.
[26] J. Rodríguez-Carvajal, Recent advances in magnetic structure determination by neutron powder diffraction, Physica B 192 (1–2) (1993) 55–69, https://doi.org/10.1016/0921-4526(93)90108-I.

[27] J.P. Schupsky, M. Guo, B. Blanpain, M. Müller, The impact of sample homogeneity, crucible material, and oxygen partial pressure on the crystallization of Fe-rich oxidic slag in CLSM experiments, J. Sustain. Metall. 6 (2) (2020) 216–226, https://doi.org/10.1007/s40831-020-00262-x.
[28] N.M. Piatak, M.B. Parsons, R.R. Seal, Characteristics and environmental aspects of slag: a review, Appl. Geochem. 57 (2015) 236–266, https://doi.org/10.1016/j.apgeochem.2014.04.009.
[29] T. Revathi, R. Jeyalakshmi, XPS, ^{29}Si, ^{27}Al, ^{11}B MAS NMR, ATR-IR and FESEM characterization of geopolymer based on borax modified water glass activated Fly ash-GGBS blend, Mater. Res. Express 6 (8) (2019), https://doi.org/10.1088/2053-1591/ab255e.
[30] G.R. Choppin, P. Pathak, P. Thakur, Polymerization and complexation behavior of silicic acid: a review, Main Group Met. Chem. 31 (1–2) (2008) 53–72, https://doi.org/10.1515/MGMC.2008.31.1-2.53.
[31] D.J. Belton, O. Deschaume, C.C. Perry, An overview of the fundamentals of the chemistry of silica with relevance to biosilicification and technological advances, FEBS J. 279 (10) (2012) 1710–1720, https://doi.org/10.1111/j.1742-4658.2012.08531.x.
[32] I. Gunnarsson, S. Arnórsson, Amorphous silica solubility and the thermodynamic properties of $H_4SiO_4^\circ$ in the range of 0° to 350°C at P_{sat}, Geochim. Cosmochim. Acta 64 (13) (2000) 2295–2307, https://doi.org/10.1016/S0016-7037(99)00426-3.
[33] D.W. Oxtoby, H.P. Gills, L.J. Butler, Principles of Modern Chemistry, Cengage Learning, 2012.
[34] S. Hong, S. Moon, J. Cho, A.-H.A. Park, Y. Park, Effects of Mg ions on the structural transformation of calcium carbonate and their implication for the tailor-synthesized carbon mineralization process, J. CO_2 Util. 60 (2022), https://doi.org/10.1016/j.jcou.2022.101999.
[35] M.M.H. Al Omari, I.S. Rashid, N.A. Qinna, A.M. Jaber, A.A. Badwan, Chapter Two – Calcium Carbonate, Profiles of Drug Substances, Excipients and Related Methodology, Academic Press, 2016, https://doi.org/10.1016/bs.podrm.2015.11.003.
[36] H. Du, E. Amstad, Water: how does it influence the $CaCO_3$ formation? Angew. Chem. Int. Ed. 59 (5) (2020) 1798–1816, https://doi.org/10.1002/anie.201903662.
[37] F.C. Meldrum, S.T. Hyde, Morphological influence of magnesium and organic additives on the precipitation of calcite, J. Cryst. Growth 231 (4) (2001) 544–558, https://doi.org/10.1016/S0022-0248(01)01519-6.